Chapter 2
New Wavelength Generation Based on PCF with Two Zero-Dispersion Wavelengths (TZDWs)

2.1 Multipole Method

Since the PCF has flexible cladding structures, the simulation method for conventional optical fibers cannot be used for the evaluation of the PCF characteristics accurately. In recent years, several methods have been developed to improve the numerical precision, such as the plane wave expansion method, beam propagation method, finite element method, and multipole method. In this thesis, we mainly use the multipole method to estimate the fiber performances.

Compared with other methods, the limited cladding structure is considered in the multipole algorithm, which is especially suitable for the microstructured fibers with circle air holes distributed in the cladding. The calculation about the mode-propagation constant for the PCFs with complex structure can be finished more accurately and faster than other methods.

In the multipole method, every air hole in the cladding is considered as a scattering cell. The electromagnetic field components can be expressed by the Bessel functions in the cylindrical coordinate system. The solution of the Helmholtz equation can be obtained by using the boundary conditions. The longitudinal component of the electric field in the nth air hole can be expressed as follows [1, 2]:

$$E_z = \sum_{m=-\infty}^{\infty} a_m^{(n)} J_m\left(k_\perp^i r_n\right) \exp(\mathrm{i}m\varphi_\mathrm{n}) \exp(i\beta z) \tag{2.1}$$

The longitudinal component of the electric field in the substrate material around the nth air hole can be expressed as follows:

$$E_z = \sum_{m=-\infty}^{\infty} \left[b_m^{(n)} J_m\left(k_\perp^e r_n\right) + c_m^{(n)} H_m^n\left(k_\perp^e r_n\right) \right] \times \exp(\mathrm{i}m\phi_\mathrm{n}) \exp(i\beta z) \tag{2.2}$$

L. Zhang, *Ultra-Broadly Tunable Light Sources Based on the Nonlinear Effects in Photonic Crystal Fibers*, Springer Theses,
DOI 10.1007/978-3-662-48360-2_2

where

$$k_{\perp}^{i} = (k_0^2 n_i^2 - \beta^2)^{1/2}\ k_{\perp}^{e} = (k_0^2 n_e^2 - \beta^2)^{1/2} \tag{2.3}$$

where $n_i = 1$ denotes the refractive index of the air, n_e denotes the refractive index of the fused silica, $k_0 = 2\pi/\lambda$ is used to express the wave numbers in the free space, and β denotes the mode-propagation constant. The magnetic field components have the similar expression with the electric field components. The coefficients of a_m, b_m, and c_m can be obtained by using the boundary condition of the electromagnetic field. The effective refractive index n_{eff} and the effective mode area A_{eff} can be obtained by using the expression between the mode-propagation constant and the wave numbers in the free space $\beta = n_{\text{eff}} k_0$. Then, the nonlinear coefficient, group velocity dispersion, loss, and birefringence can be obtained.

2.2 Parametric Amplification Based on PCF with TZDW

2.2.1 The Design and Fabrication of the PCF with TZDW

The ZDW is an important parameter for optical fibers. When the pump is located near the ZDW, the nonlinear effects can be increased remarkably, and the optical parametric components can be generated easily. Fiber-based optical parametric generation is the cornerstone of the FOPA, FOPO, and all-optical wavelength converter. The ZDW of the traditional nonlinear fibers (highly-nonlinear fibers, dispersion-shifted fibers, and the highly-nonlinear dispersion-shifted fibers) is located around 1550 nm, and it can be tuned only in a very small wavelength range, which is determined by the fiber structure and the fabricated process. Since the PCF has flexible cladding and core structures, the ZDW can be tuned to nearly "any" wavelength in the transparent window. It means that the optical parametric components can be generated from visible to the infrared band flexibly.

Fiber-based optical parametric generation, also named as modulation instability, refers to the phenomenon that signals from the spontaneous emission are amplified by the pump wave. The shape and the distribution of the optical parametric spectral components are closely related to the nonlinear effect of FWM. Marhic et al. [3] reported a widely tunable optical parametric generation with the anti-Stokes spectral components around 1350 nm in a highly-nonlinear dispersion-shifted fiber pumped in the normal dispersion wavelength regime by a tunable diode laser. Wong et al. demonstrated the evolution of the optical parametric spectral components versus the pump wavelength by using a quasi-continuous wave laser source. When the PCF is pumped near the ZDW, a wide-band parametric spectrum can be formed. When the PCF is pumped in the normal dispersion wavelength regime, two narrow parametric bands can be generated far from the pump [4]. Harvey et al. demonstrated that the parametric spectral components can be tuned largely by adjusting the polarization state of the pump in a birefringent PCF [5].

It is clear that the FWM optical parametric spectral components can be easily generated by pumping the PCF near the ZDW. Andersen et al. obtained a widely tuned optical parametric generation in a PCF with two zero-dispersion wavelengths (TZDWs) by using a Ti: sapphire laser as the pump source [6]. Tuan et al. [7] theoretically predicted that largely tuned parametric components can be generated in a PCF with four ZDWs. The largely tuned optical parametric generation has a lot of applications, such as new wavelength laser source, large span wavelength converter, and entangled pair-photon source. In this section, we would like to design and fabricate a PCF with TZDW for the realization of large span optical parametric generation.

The PCF structure is designed by using the multipole method. In order to ensure the precision during the fabrication, hexagonal cladding structures are adopted. The fused silica is used as the substrate material. The designed cross-sectional structure of the PCF is shown in Fig. 2.1. The pitch of the air holes is 1.15 μm, the diameter of the air holes is 0.75 μm, and the diameter of the fiber core is 1.55 μm. The effective refractive index and the effective mode area at different wavelength can be calculated by using the multipole method. Based on the relation between the refractive index and the dispersion, the group velocity dispersion of the fundamental mode can be obtained, which is shown in Fig. 2.2. The two ZDWs are located at 701 and 1115 nm, respectively.

When a single-longitudinal-mode laser is used as the pump source, the frequencies and the propagation constants of the two pump photons are the same.

$$\omega_1 = \omega_2 = \omega_p \tag{2.4}$$

$$\beta_1 = \beta_2 = \beta_p \tag{2.5}$$

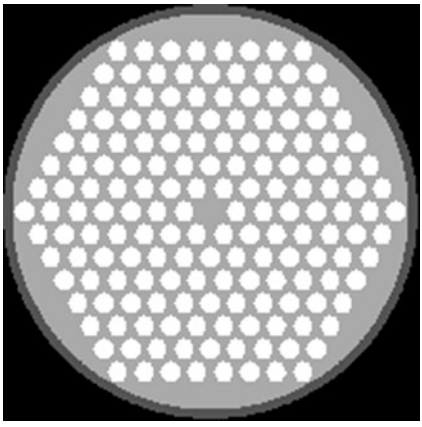

Fig. 2.1 The cross section of the designed PCF

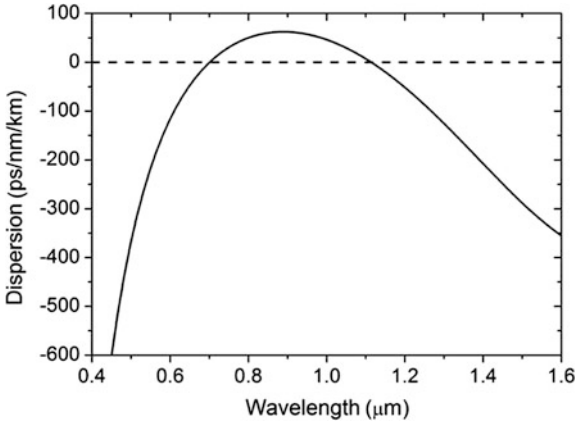

Fig. 2.2 The group velocity dispersion for the designed PCF with TZDW

The phase-matching condition for the single pump case can be expressed as follows:

$$2\omega_p = \omega_s + \omega_i \tag{2.6}$$

$$\Delta k = \Delta\beta = \beta_s + \beta_i - 2\beta_p = 0 \tag{2.7}$$

The propagation constant can be calculated by the equation of $\beta = n\omega/c$. The phase-matching condition can be predicted by a combination of the Eqs. (2.6) and (2.7), which is shown in Fig. 2.3 plotted by pump wavelength on the horizontal axis and the wavelengths of the signal and idler on the vertical axis. In the figure, the blue line represents the signal and the red line represents the idler. When the pump is located at 780 nm, the phase-matched signal and idler arise at the telecommunication band of 1550 nm and the visible band of 521 nm, respectively, which is denoted by the purple line in the figure.

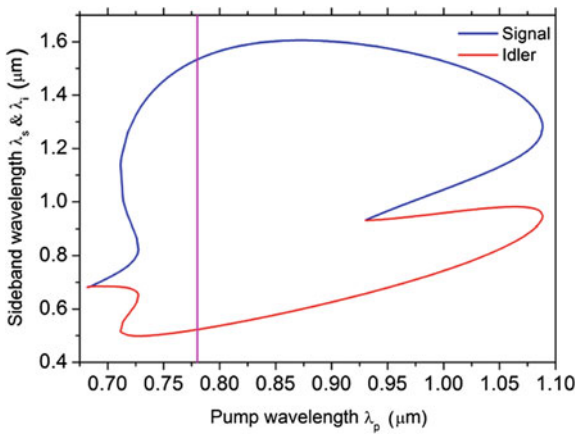

Fig. 2.3 The phase-matching profile for the designed PCF with TZDW

The designed PCF is featured with a small core, which can provide a high nonlinearity. The microstructure of the designed PCF introduces a lot of challenges to the technical fabrication. The group of Prof. Jinyan Li in Huazhong University of Science and Technology fabricated this fiber for us successfully by overcoming lots of difficulties. The SEM image of the cross section of the fabricated PCF is shown in Fig. 2.4. According to the fiber parameters extracted from the SEM image, the dispersion property is calculated, and the TZDWs are located at 723 and 1363 nm, respectively, as shown in Fig. 2.5. The nonlinear coefficient is calculated to be 160 km^{-1} W^{-1} at 800 nm.

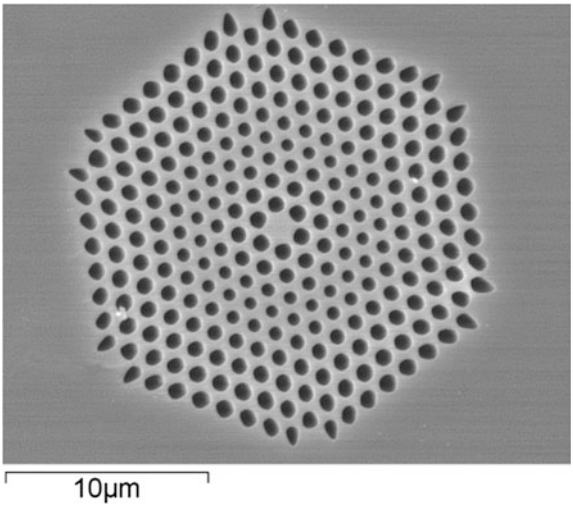

Fig. 2.4 The SEM image of the cross section of the fabricated PCF with TZDW

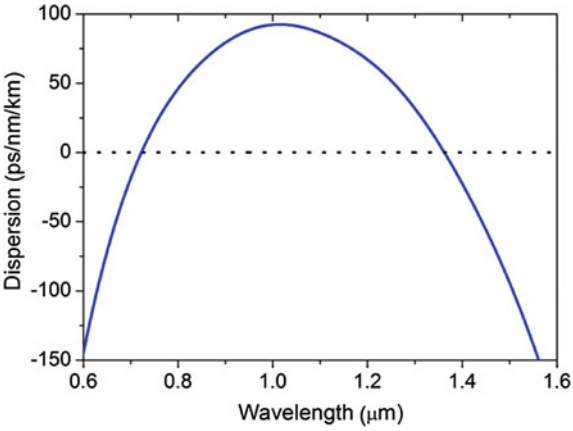

Fig. 2.5 The calculated dispersion for the fabricated PCF

2.2.2 The Relationship Between the Optical Parametric Spectrum and the Pump Wavelength

In order to accurately simulate the optical parametric generation, the contribution of the nonlinear effect to the phase matching should be considered, and the phase-matching condition equation should be modified accordingly. For the single pump case, the revised phase-matching condition can be expressed as follows:

$$\kappa = \Delta\beta + 2\gamma P = \beta_s + \beta_i - 2\beta_p + 2\gamma P = 0 \tag{2.8}$$

where P denotes the pump power. With the propagation constants β_s and β_i Taylor expanded around the pump frequency, Eq. (2.9) can be written as follows:

$$\kappa = \Omega^2\beta_2 + \frac{1}{12}\Omega^4\beta_4 + \frac{1}{360}\Omega^6\beta_6 + \cdots + 2\gamma P = 0 \tag{2.9}$$

where Ω denotes the frequency detuning between the pump and the signal. It can be seen that only the even-order dispersion and the nonlinearity have influence on the phase-matching condition. When the linear phase mismatch is located in the region of $-4\gamma P < \Delta\beta < 0$, a nonzero parametric gain can be obtained. It requires that the group velocity dispersion parameter $\beta^{(2)}$ at the pump wavelength is approximately in the range of:

$$-\frac{4\gamma P}{\Omega^2} - \frac{\beta^{(4)}\Omega^2}{12} < \beta^{(2)} < -\frac{\beta^{(4)}\Omega^2}{12} \tag{2.10}$$

where $\beta^{(4)}$ is the fourth derivative of the propagation parameter β with respect to the pump wavelength. When $\beta^{(4)} < 0$, the parametric gain can be obtained by pumping the fiber in the normal dispersion region of:

$$\beta^{(2)} < -\beta^{(4)}\Omega^2/12 \tag{2.11}$$

which is near the ZDW, or by pumping in the anomalous dispersion region of:

$$\beta^{(2)} > -4\gamma P/\Omega^2 - \beta^{(4)}\Omega^2/12 \tag{2.12}$$

when $\beta^{(4)} > 0$, the parametric gain can be obtained by pumping the fiber in the anomalous dispersion region of:

$$-4\gamma P/\Omega^2 - \beta^{(4)}\Omega^2/12 < \beta^{(2)} < -\beta^{(4)}\Omega^2/12 \tag{2.13}$$

If the pump wave locates in the normal dispersion region of $\beta^{(2)} > |\beta^{(4)}\Omega^2/12|$, which is far from the ZDW or in the huge negative dispersion region of $\beta^{(2)} < -4\gamma P/\Omega^2 - |\beta^{(4)}\Omega^2/12|$, the parametric spectral components cannot be observed [8].

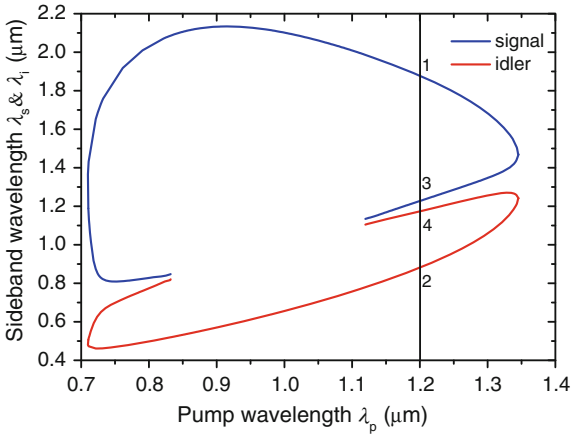

Fig. 2.6 The phase-matching contour for the nonlinear mismatch term of $\gamma P = 0$. Reprinted from Ref. [8], copyright © 2013, with permission from Elsevier

The phase-matching contour for the fundamental mode of the PCF with nonlinear mismatch term $\gamma P = 0$ is shown in Fig. 2.6. The range of the pump wavelength, in which phase-matched signal and idler pair exist, is from 710 to 1346 nm, beginning at the normal dispersion regime near the first ZDW of 723 nm, and ending at the anomalous dispersion regime close to the second ZDW of 1363 nm. For each pump wave in the regions from 710 to 832 nm and from 1120 to 1346 nm, two groups of phase-matched signal and idler pairs exist. For example, for the pump wavelength of 1200 nm, the outer pair of the phase-matched points is marked with 1 and 2, and the inner pair of the phase-matched points is marked with 3 and 4, as shown in the vertical solid line on Fig. 2.6. For each pump wave in the region from 832 to 1120 nm, only one group of phase-matched signal and idler pair exists, and the signal and the idler bands have a large interval. Figure 2.7 shows the evolution of the phase-matched sidebands versus the pump wavelength with different pump power. The black slash shows the location of the pump wavelength in the vertical

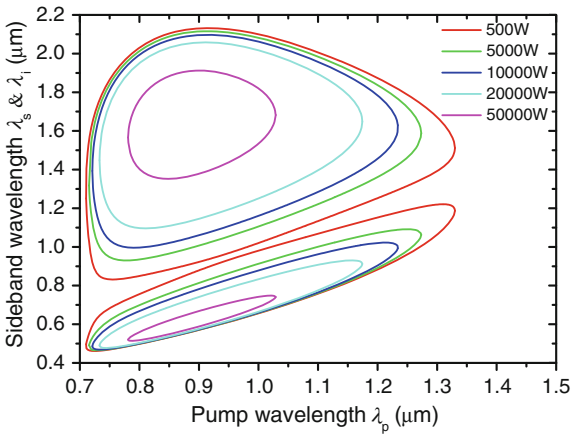

Fig. 2.7 The phase-matching contours for different pump power. Reprinted from Ref. [8], copyright © 2013, with permission from Elsevier

coordinate. The curves above the slash indicate the wavelengths of the signal sidebands, and the curves below the slash indicate the wavelengths of the idler sidebands. When the peak pump power is 500 W, for each pump wavelength in the region from 711 to 1330 nm, two groups of phase-matched signal and idler pairs exist. The inner and outer phase-matched pairs constitute a ring shape on each side of the slash of the pump wavelength. With the peak pump power increased, the nonlinear phase mismatch will seriously affect the phase-matching condition. The pump wavelength region in which the phase-matched waves pair can appear becomes smaller. The frequency detuning of the inner pair from the pump wave increases, and the frequency detuning of the outer pair from the pump wave decreases.

The gain bandwidth is a critical parameter to the parametric amplification. The frequencies distributed in the region of $-4\gamma P < \Delta\beta(\Omega) < 0$ will experience a nonzero gain. Figure 2.8 shows the phase-matching contours for the fundamental mode of the PCF when the linear phase mismatch $\Delta\beta$ equals to $-4\gamma P$, $-2\gamma P$ and zero, respectively, and the peak pump power P is 20,000 W. For a given pump wavelength, the gain band covers the wavelengths that satisfy the condition of $-4\gamma P < \Delta\beta(\Omega) < 0$. The phase-matching curve with $\Delta\beta = -2\gamma P$ indicates the signals and idlers with the maximal gain. Based on the profiles of the gain spectrum, the pump wavelengths are divided into six regions. In the region 1, for a given pump wave, there are four separated gain bands, corresponding to the signal and idler gain bands of the inner and outer pairs, respectively. For example, with the pump wavelength of 800 nm, the four gain bands are a, b, c, and d, respectively, which are marked in the Fig. 2.10. In the region 2, for a given pump, the signal and idler bands of the inner pair are connected to each other, and a broad band is formed near the pump wavelength except for two separated signal and idler bands of the outer

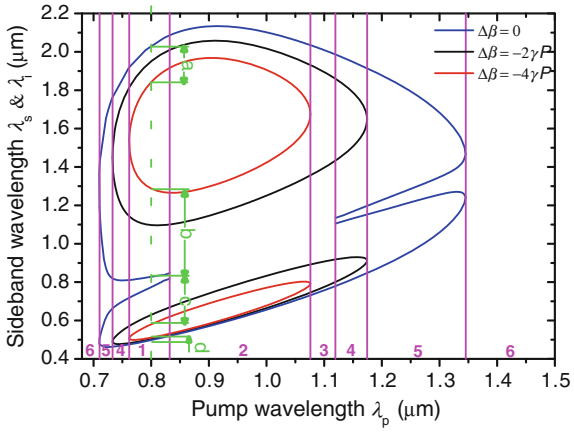

Fig. 2.8 The Phase-matching contours for the high group-index mode of the PCF with the linear phase mismatch $\Delta\beta$ of $-4\gamma P$, $-2\gamma P$ and zero, respectively, when the pump power is 20,000 W. Reprinted from Ref. [8], copyright © 2013, with permission from Elsevier

pair. In the region 3, for a given pump, the four gain bands are all connected to each other and form a superbroad gain band similar to a supercontinuum spectrum. In the region 4, for a given pump, the idler or signal of the outer and inner gain bands are combined together. Either the signal or the idler band includes two gain peaks since two fulfilled phase-matching wavelengths are existed. In the region 5, the fulfilled phase-matched wavelengths do not exist, and the parametric gain is very weak. The region 6 belongs to zero gain region, and no parametric gain exists. It can be predicted that, according to band gain contours, various parametric gain shapes can be obtained by adjusting the pump wavelength.

2.2.3 *The Optical Parametric Generation in a PCF with TZDW*

The optical parametric spectra are measured for the PCF with TZDW. The experimental setup is shown in Fig. 2.9. Experimentally, a Ti: sapphire pulse laser can emit a pulse train with the full width at half maximum (FWHM) of 130 fs, at the repetition rate of 76 MHz. The pump pulse train is coupled into 1.0-m PCF mentioned above through a 40 × microscope objective lens with the numerical aperture of 0.65. The central wavelength of the pump wave is set to be 800 nm. The pump power can be adjusted by a neutral-density filter wheel. The light emitting from the fiber is collimated by a 40 × microscope objective lens and then sent to two optical fiber spectrometers (Avaspec-2048-2 and Avaspec-NIR-256-2.5) with the measurement scopes from 200 to 1100 nm and from 900 to 2500 nm.

Since the signal band distributing in the wavelength region of 1000–2200 nm, a suitable signal source is not accessible. We used amplified spontaneous emission (ASE) from the pump laser as the seed source and inferred the FOPA gain spectrum from the measurement of the output ASE spectrum. The experimentally observed spectra for the peak pump power of 20,000 W and the pump wavelengths of 760, 800 and 815 nm are shown in Fig. 2.10. The idler bands are shown in Fig. 2.10a, c, and e, in which two gain bands in visible region can be clearly seen. When the pump is operated at 800 nm, the region of 550–730 nm corresponds to the idler wave of the inner pair (IWIP) of the sideband, and the region of 410–501 nm corresponds to the idler wave of the outer pair (IWOP) of the sideband. When the pump wavelength increases, both the IWIP and IWOP move to the longer

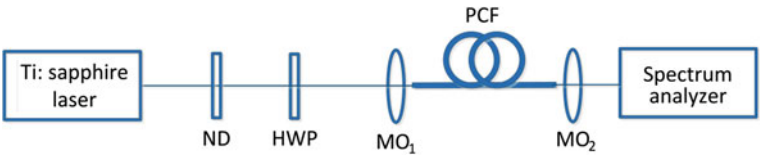

Fig. 2.9 The experimental setup

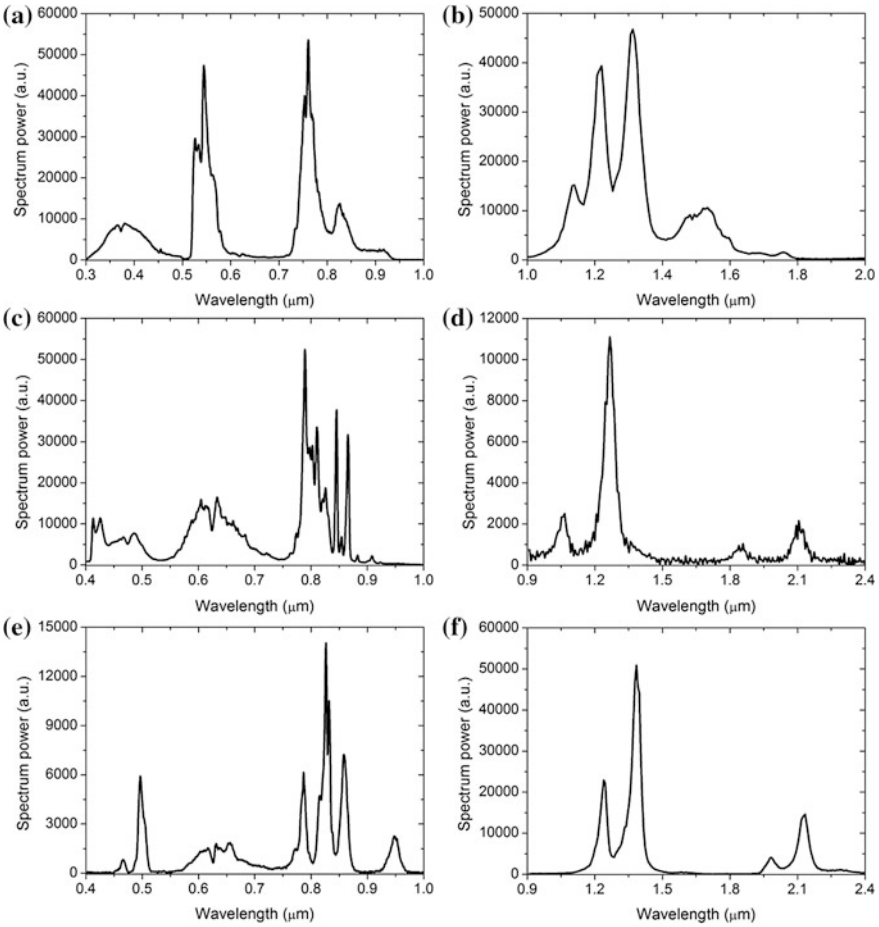

Fig. 2.10 The observed output spectra of the idler waves, with the pump wavelengths of **a** 0.76 μm, **c** 0.8 μm, and **e** 0.815 μm, respectively. The observed output spectra of the signal waves, with the pump wavelengths of **b** 0.76 μm, **d** 0.8 μm, and **f** 0.815 μm, respectively. The peak pump power is set at P = 20,000 W. Reprinted from Ref. [8], copyright © 2013, with permission from Elsevier

wavelength, which is shown in Fig. 2.11. In particular, when the pump wavelength is 760 nm, the idler wave extends down to the ultraviolet region of 300 nm. The signal waves are shown in Fig. 2.10b, d, and f. Two gain bands corresponding to the signal waves of the inner and outer pairs (SWIP and SWOP) can be observed clearly. For example, when the pump wavelength is 800 nm, the two gain bands distribute in bands of 1010–1320 nm and 1805–2160 nm, respectively. Each band has two peaks resulted from the birefringence of the PCF, since only one half-wave plate is used and the polarization state of pump is not aligned properly with the principle axis of the PCF. Theoretically, a half-wave plate and two quarter-wave

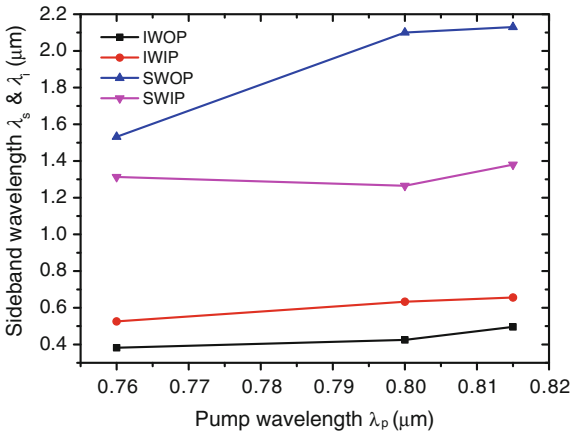

Fig. 2.11 Sideband wavelength of the two pairs of FWM versus the pump wavelength, the peak pump power is set at 20,000 W. Reprinted from Ref. [8], copyright © 2013, with permission from Elsevier

plates should be used simultaneously so that all the polarization states can be reached. The evolution of the signal band versus the pump wavelength is also shown in Fig. 2.11. When the pump wavelength is 815 nm, the signal band extends to the mid-infrared region of 2190 nm. The two pairs of gain bands are approximately in agreement with the simulation results in Fig. 2.7.

In order to further study the evolution of the two pairs FWM gain bands versus the propagation distance, we simulate the sech^2 pulses with peak power of 20,000 W and 130 fs FWHM propagating in 1-m PCF using the split-step Fourier method to solve the generalized nonlinear Schrödinger equation [9]. The spectral evolution is shown in Fig. 2.12. It is clear that two pairs of sideband are generated at the propagation distance about 3 mm. As shown in Fig. 2.12, the outer pair of FWM gain bands is composed of A and B, and the inner pair is composed of C and D. The wavelengths of them remain relatively fixed with the increasing of the propagation distance to 1 m.

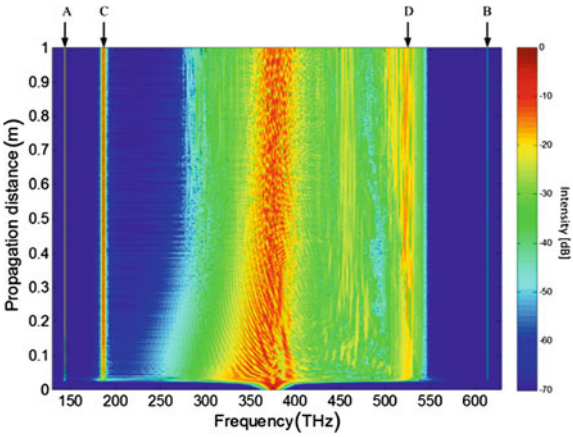

Fig. 2.12 Simulated spectral evolution of a pulse launched at 800 nm with the peak pump power of 20,000 W. Reprinted from Ref. [8], copyright © 2013, with permission from Elsevier

Reeves et al. [10] theoretically predicted that two pairs of gain bands can be existed in particular dispersion-engineered PCFs as early as 2003. This phenomenon is clearly observed in this experiment for the first time. The relationship between the optical parametric spectrum and the pump wavelength provides more effective interpretations to the SC generation.

2.3 Dispersive Wave Generation

2.3.1 The Principle of Dispersive Wave Generation

When optical pulses are transmitted in the anomalous dispersion regime, multiple solitons can be generated by the soliton fission of the pump pulse. The soliton frequency can be continuously shifted to the longer wavelength region by the intra-pulse Raman scattering. When the solitons are perturbed by third-order and higher order dispersion, the energy can be transferred to the dispersive waves (DWs) located in the normal dispersion regime [11]. The DW is also named as Cherenkov radiation (CR) or nonsolitonic radiation (NSR). The SC can be broadened to the shorter and longer wavelength regions by the DW [12–16]. Tunable DW in the wavelength region from 485 to 600 nm has been reported in a PCF [17, 18]. By using a variety of PCFs with different group velocity dispersion, the DW wavelength can even be extended to UV region [19–21]. Based on a PCF with TZDW, large amplitude DW near 1600 nm have been generated in the longer normal dispersion wavelength region, which is beyond the second ZDW [22]. The DW at the wavelength of 1720 nm has been obtained experimentally by Schreiber et al. [14].

The DW generation requires that the phase-matching condition of the DW propagates with the same phase velocity as that of the soliton should be satisfied. The phase shift of soliton can be expressed as follows:

$$\phi(\omega_s) = \beta(\omega_s)z - \omega_s(z/v_g) + \frac{1}{2}\gamma P_s z \tag{2.14}$$

where ω_s is the soliton frequency, v_g is the group velocity of the soliton, and P_s is the soliton peak power. The phase shift of the DW can be expressed as follows:

$$\phi(\omega_d) = \beta(\omega_d)z - \omega_d(z/v_g) \tag{2.15}$$

where ω_d is the DW frequency. After expanding the mode-propagation constant of the DW in a Taylor series about the soliton frequency, the phase-matching condition can be expressed as follows:

$$\sum_{n\geq 2}\frac{(\omega_d-\omega_s)^n}{n!}\beta_n=\frac{\gamma P_s}{2} \tag{2.16}$$

In the qualitative analysis, the value of ω_{CR} is mainly affected by the first few terms of the left part of Eq. (2.16). When only the first two terms on the left part are taken into account, the Eq. (2.16) can be written simply as follows:

$$\frac{(\omega_d-\omega_s)^2}{2}\beta_2+\frac{(\omega_d-\omega_s)^3}{6}\beta_3=\frac{\gamma P_s}{2} \tag{2.17}$$

Physically, the right part is always positive. The soliton can be formed at the anomalous dispersion regime ($\beta_2 < 0$). When the third-order dispersion (TOD) is positive ($\beta_3 > 0$), the value of ω_{CR} is larger than that of ω_s, and the CR shifts to shorter wavelength regions. When the TOD is negative $\beta_3 < 0$, the value of ω_{CR} is smaller than that of ω_s, and the CR shifts to the longer wavelength region.

2.3.2 *Tunable DWs in the Visible Region*

In the experiment, a mode-locked Ti: sapphire femtosecond pulsed laser is used as the pump source. A highly-nonlinear PCF with TZDW is used as the nonlinear medium. The calculated dispersion parameter β_2 and the TOD parameter β_3 versus the wavelength are shown in Fig. 2.13. In the vicinity of 1025 nm, β_3 moves from positive to negative.

When the pump wave is operated at 800 nm with an average power of 70 mW, the spectrum obtained from the optical fiber spectrometer is shown in Fig. 2.14. The

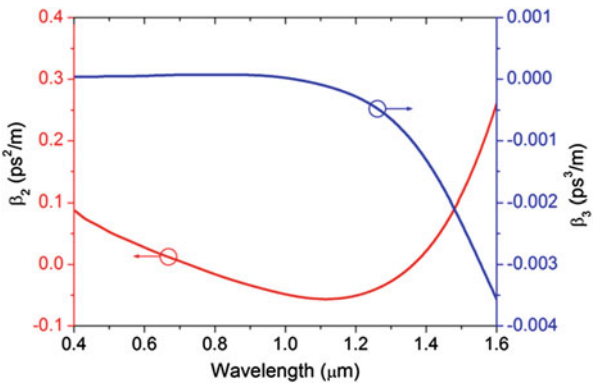

Fig. 2.13 The calculated dispersion parameter β_2 and third-order dispersion parameter β_3 for the fundamental mode of the PCF. The inset shows the scanning electron microscope (SEM) image of the cross section of the PCF

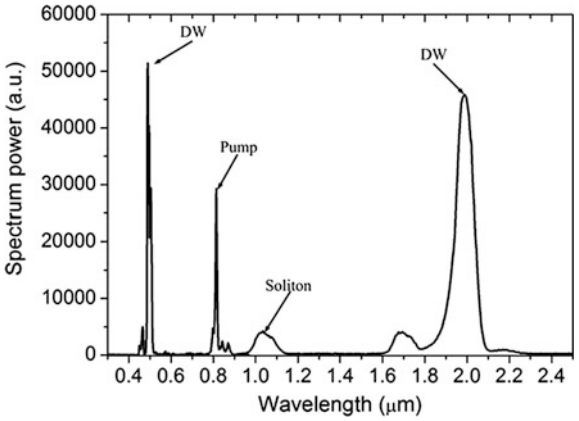

Fig. 2.14 The experimentally measured spectrum for the pump operating at 800 nm with an average power of 70 mW

soliton is firstly formed near the pump wavelength, where $\beta_3 > 0$, and the DW is generated at 498 nm based on the phase-matching condition between the soliton and DW. Then, the soliton shifts toward the longer wavelength region because of the RIFS. When the soliton approaches the second ZDW, where $\beta_3 < 0$, the DW is generated at 1986 nm. The RIFS is canceled by the spectral recoil from the generation of the DW at 1986 nm, and the soliton is stabilized in the wavelength region close to the second ZDW [23].

The wavelength of the DW in the visible region is studied by adjusting the average pump power. As shown in Fig. 2.15, with the average pump power increasing from 70 to 400 mW, the wavelength of DW can be tuned from 498 to 425 nm. The conversion efficiency is calculated, which is shown by the black line in Fig. 2.16. The conversion efficiency of the visible DW increases monotonously with the average pump power. It reaches 42 % at the average pump power of 400 mW [24].

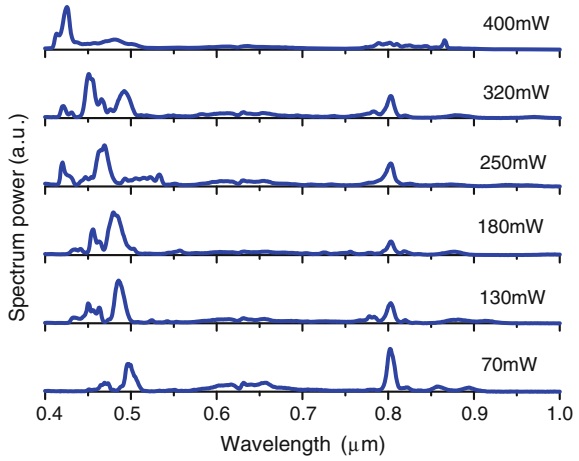

Fig. 2.15 The evolution of the DW in the visible region with the average pump power increasing from 70 to 400 mW

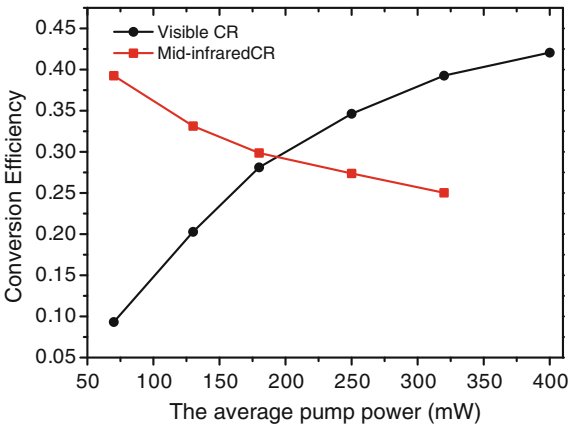

Fig. 2.16 The conversion efficiencies of the visible and mid-infrared DWs versus the average pump power

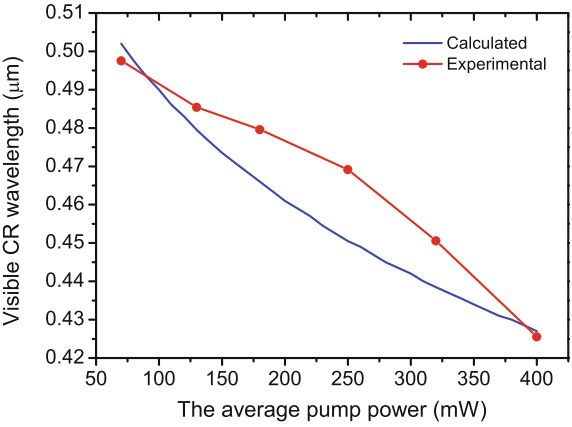

Fig. 2.17 The calculated and experimentally measured DW wavelength in the visible as a function of the average pump power

The wavelength of the DW is governed by the phase-matching condition between the DW and the soliton formed near the pump wavelength, which is in the region of $\beta_3 > 0$. Based on the phase-matching condition, the DW wavelength is predicted. In the simulation, dispersive effects up to 10th order are included. The calculated and the experimentally measured DW wavelengths versus the average pump power are shown in Fig. 2.17. The discrepancy is limited in the range of 18 nm, which is induced by the wavelength of the soliton which is set to be 800 nm in the simulation. The trend of the predicted DW wavelength evolution is a little different with that obtained in the experiment. This could be induced by the accuracy of the simulated dispersion terms. Except for the DW generation, FWM process can also happen. For each pump wavelength, two groups of phase-matched signal and idler pairs exist. The spectral component between the pump wave and the DW is considered to be generated by the FWM between the pump wave and the red-shifted fundamental soliton. The idler of the outer group of the FWM distribute in the vicinity of the DW.

2.3.3 *Tunable DWs in the Mid-infrared Region*

The wavelength of the DW in mid-infrared region can also be tuned by adjusting the average pump power. As shown in Fig. 2.18, with the average pump power increasing from 70 to 320 mW, the wavelength of the DW can be tuned from 1986 to 2279 nm. When the average pump power is 400 mW, the mid-infrared DW is not observed. This is considered to be due to that the wavelength of the mid-infrared DW exceeds the measurement scope of the optical spectrometer. The wavelength of the fundamental soliton shifts from 1035 to 1190 nm, where β_3 is always negative. The conversion efficiency of the mid-infrared DW is also shown in Fig. 2.16. For the average pump powers of 70, 130, 180, 250, and 320 mW, the conversion efficiencies are calculated to be 39, 33, 30, 27, and 25 %, respectively. The spectral component between the fundamental soliton and the DW is considered to be generated by the FWM between the pump and the DW in the visible wavelength region.

The wavelength of the DW in the mid-infrared region is governed by the phase-matching condition between the DW and the fundamental soliton, which is stabilized in the region of $\beta_3 < 0$. The wavelength evolution of the DW is predicted by the phase-matching condition. The calculated and experimentally measured DW wavelengths versus the average pump power are shown in Fig. 2.19. The discrepancy is limited in the range of 26 nm, which is induced by the wavelength of the stabilized soliton which is set to be 1100 nm in the simulation [25].

Tunable DWs have been obtained in the mid-infrared normal dispersion wavelength regime by using a PCF with TZDW as the nonlinear medium. Mid-infrared light source can be used in many applications, such as the integrated silicon nanophotonics circuit communication systems, free-space communication, and biophotonics. The investigation about the high-efficient mid-infrared DW generation will promote the development of the related areas.

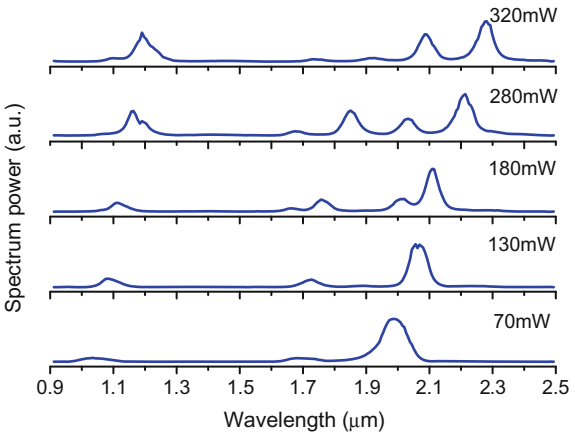

Fig. 2.18 The evolution of the DW in the mid-infrared region with the average pump power increasing from 70 to 320 mW

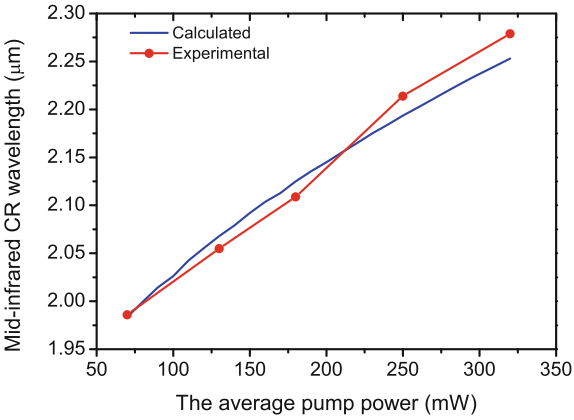

Fig. 2.19 The calculated and experimentally measured mid-infrared DW wavelengths as a function of the average pump power

2.4 Ultraviolet Generation Based on Cross-Phase Modulation in PCF with TZDW

Supercontinuum (SC) spanning from the visible to the near-infrared region has been widely investigated and utilized in many fields [26]. Nonetheless, recently many efforts have been devoted to extend the SC to mid-infrared and ultraviolet (UV) regions [27, 28]. Light source in the UV region is urgently needed in the applications of fluorescence microscopy, spectroscopy, and biomedical photonics. DW generation and four-wave mixing (FWM) are effective ways to extend the SC to short wavelength region. However, both of them require the phase-matching condition, which is difficult to fulfill in the UV wavelength region. UV SC had been generated by pumping a PCF with a picosecond microchip laser at 355 nm. However, due to the large normal dispersion at UV region and the effect of Raman-induced frequency shift, the spectrum is mainly extends to longer wavelength regions [29].

Except for the DW generation and FWM, cross-phase modulation (XPM) is also an effective way to extend the SC to shorter wavelength regions. In an experiment, dual-frequency (1064 and 532 nm) pulsed pump waves are simultaneously coupled into a photonic crystal fiber (PCF). The Raman-induced frequency shift of the pulse at 532 nm is inhibited by the XPM induced by the pulse at 1064 nm, and the SC extends to shorter wavelength region of 350 nm [30]. SC has been extended to short wavelength region of 300 nm by the effect of XPM between the anti-Stokes signal at 550 nm and the pump pulse at 830 nm [31].

When the PCF with TZDW is pumped by a Ti: Sapphire pulse at 800 nm, one of the anti-Stokes signals appears in the region from 400 to 550 nm. The calculated relative group delay β_1 with respect to the pump wavelength of 800 nm and the dispersion parameter β_2 versus the wavelength are shown in Fig. 2.20. It is predicted that XPM between the anti-Stokes signal and the Raman soliton generated by the pump can be occurred.

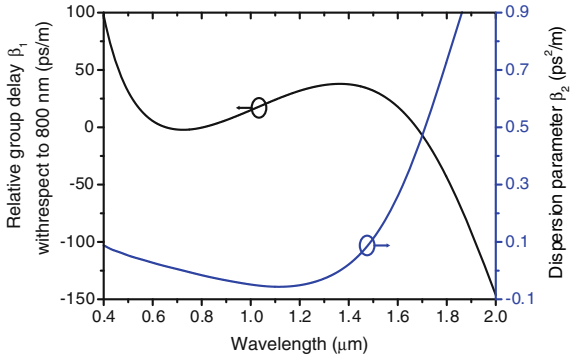

Fig. 2.20 Variations of the relative group delay β_1 and the dispersion parameter β_2 with respect to the wavelength. Reprinted from Ref. [32], copyright © OSA 2013, with permission from OSA

The experimental spectra for the average pump power of 200, 300, and 400 mW are shown in Fig. 2.21 For the input average pump power of 200 mW, the inner and outer anti-Stokes signals are observed at 550–750 nm and 400–550 nm, respectively. This is consistent with the simulation results about the two pairs of FWM. According to the relative group delay in Fig. 2.20, the outer anti-Stokes signal has a lower group velocity than the pump soliton. As the Raman-induced frequency shift, the pump soliton shifts to longer wavelengths, and the group velocity slows down. Then, the soliton overlaps with the outer anti-Stokes signal temporally. The anti-Stokes signal is affected by the XPM induced by the pump soliton. The SC is extended to the UV region of 200–400 nm. As the input power is increased, the frequency component in the UV region of 200–400 nm tends to become flat [32]. The experimental scene is shown in Fig. 2.22. Figure 2.23 shows the optical spot of the fundamental mode at the output.

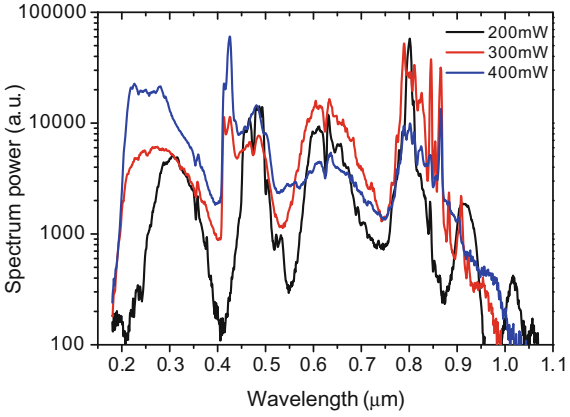

Fig. 2.21 The experimental spectra for the average pump powers of 200, 300, and 400 mW. Reprinted from Ref. [32], copyright © OSA 2013, with permission from OSA

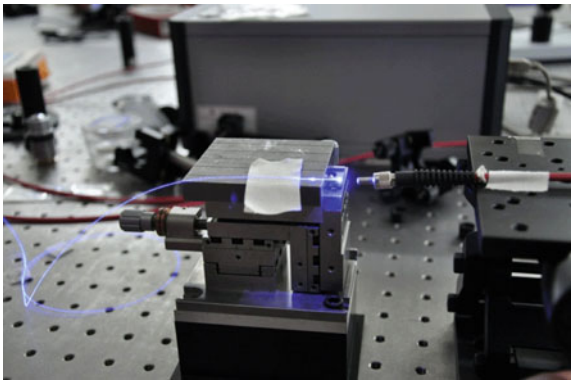

Fig. 2.22 The experimental scene of the XPM

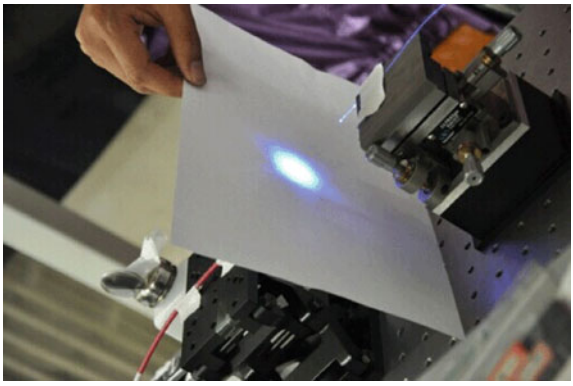

Fig. 2.23 The optical spot of the fundamental mode at the output

2.5 Conclusion

In this chapter, we first investigate the relationship between the FWM parametric spectrum and the dispersion, nonlinear coefficient, and pump wavelength. A PCF with TZDW is carefully designed and fabricated. The parametric spectra in this PCF are measured by using a Ti: sapphire laser as the pump. Two pairs of large span parametric sidebands are observed, and the sideband in mid-infrared region can be extended to 2190 nm.

Second, the DW generation is investigated in this PCF. In the experiment, visible and mid-infrared DWs can be generated simultaneously by pumping in the anomalous dispersion regime between the TZDWs. The visible DW can be generated from 498 to 425 nm, and the mid-infrared DW can be tuned from 1986 to 2279 nm.

Third, the XPM effect is investigated in this PCF. The FWM and DW generation effects can emit an anti-Stokes signal in the blue–violet region. Due to the XPM between the anti-Stokes signal and the Raman soliton, the SC can extend to the ultraviolet region of from 200 to 400 nm.

References

1. T.P. White, B.T. Kuhlmey, R.C. McPhedran, D. Maystre, G. Renversez, C. Martijn de Sterke, L.C. Botten, Multipole method for microstructured optical fibers. I. Formulation. J. Opt. Soc. Am. B **19**(10), 2322–2330 (2002)
2. B.T. Kuhlmey, T.P. White, G. Renversez, D. Maystre, L.C. Botten, C. Martijn de Sterke, R.C. McPhedran, Multipole method for microstructured optical fibers. II. Implementation and results. J. Opt. Soc. Am. B **19**(10), 2331–2340 (2002)
3. M.E. Marhic, K.K.Y. Wong, L.G. Kazovsky, Wide-band tuning of the gain spectra of one-pump fiber optical parametric amplifiers. IEEE J. Sel. Top. Quant. Electron **10**(5), 1133–1141 (2004)
4. G. Wong, A. Chen, S.G. Murdoch, R. Leonhardt, J.D. Harvey, N.Y. Joly, J.C. Knight, W.J. Wadsworth, P.J. Russell, Continuous-wave tunable optical parametric generation in a photonic-crystal fiber. J. Opt. Soc. Am. B **22**(11), 2505–2511 (2005)
5. J.D. Harvey, R. Leonhardt, S. Coen, G.K.L. Wong, J.C. Knight, W.J. Wadsworth, P. Russell, Scalar modulation instability in the normal dispersion regime by use of a photonic crystal fiber. Opt. Let. **28**(22), 2225–2227 (2003)
6. T.V. Andersen, K.M. Hilligsøe, C.K. Nielsen, J. Thøgersen, K.P. Hansen, S.R. Keiding, J.L. Larsen, Continuous-wave wavelength conversion in a photonic crystal fiber with two zero-dispersion wavelengths. Opt. Express **12**(17), 4113–4122 (2004)
7. T.H. Tuan, T. Cheng, K. Asano, Z. Duan, W. Gao, D. Deng, T. Suzuki, Y. Ohishi, Optical parametric gain and bandwidth in highly nonlinear tellurite hybrid microstructured optical fiber with four zero-dispersion wavelengths. Opt. Express **21**(17), 20303–20312 (2013)
8. L. Zhang, S.-G. Yang, Y. Han, H.-W. Chen, M.-H. Chen, S.-Z. Xie, Optical parametric generation with two pairs of gain bands based on a photonic crystal fiber. Opt. Commun. **300**, 22–26 (2013)
9. G.P. Agrawal, *Nonlinear Fiber Optics* (Springer, Berlin Heidelberg, 2000)
10. W.H. Reeves, D.V. Skryabin, F. Biancalana, J.C. Knight, P.J. Russell, F.G. Omenetto, A. Efimov, A.J. Taylor, Transformation and control of ultrashort pulses in dispersion-engineered photonic crystal fibres. Nature **424**(6948), 511–515 (2003)
11. N. Akhmediev, M. Karlsson, Cherenkov radiation emitted by solitons in optical fibers. Phys. Rev. A **51**(3), 2602–2607 (1995)
12. B.H. Chapman, J.C. Travers, S.V. Popov, A. Mussot, A. Kudlinski, Long wavelength extension of CW-pumped supercontinuum through soliton-dispersive wave interactions. Opt. Express **18**(24), 24729–24734 (2010)
13. D.R. Austin, C.M. de Sterke, B.J. Eggleton, T.G. Brown, Dispersive wave blue-shift in supercontinuum generation. Opt. Express **14**(25), 11997–12007 (2006)
14. T. Schreiber, T. Andersen, D. Schimpf, J. Limpert, A. Tünnermann, Supercontinuum generation by femtosecond single and dual wavelength pumping in photonic crystal fibers with two zero dispersion wavelengths. Opt. Express **13**(23), 9556–9569 (2005)
15. V. Husakou, J. Herrmann, Supercontinuum generation in photonic crystal fibers made from highly nonlinear glasses. Appl. Phys. B Lasers Opt. **77**(2–3), 227–234 (2003)
16. M. Frosz, P. Falk, O. Bang, The role of the second zero-dispersion wavelength in generation of supercontinua and bright-bright soliton-pairs across the zero-dispersion wavelength. Opt. Express **13**(16), 6181–6192 (2005)
17. G. Chang, L.J. Chen, F.X. Kärtner, Highly efficient Cherenkov radiation in photonic crystal fibers for broadband visible wavelength generation. Opt. Let. **35**(14), 2361–2363 (2010)
18. J. Yuan, X. Sang, C. Yu, Y. Han, G. Zhou, S. Li, L. Hou, Highly efficient and broadband Cherenkov radiation at the visible wavelength in the fundamental mode of photonic crystal fiber. IEEE Photon. Technol. Lett. **23**(12), 786–788 (2011)
19. H. Tu, S.A. Boppart, Optical frequency up-conversion by supercontinuum-free widely unable fiber optic Cherenkov radiation. Opt. Express **17**(12), 9858–9872 (2009)

20. H. Tu, S.A. Boppart, Ultraviolet-visible non-supercontinuum ultrafast source enabled by switching single silicon strand-like photonic crystal fibers. Opt. Express **17**(20), 17983–17988 (2009)
21. S.P. Stark, A. Podlipensky, N.Y. Joly, P.J. Russell, Ultraviolet-enhanced supercontinuum generation in tapered photonic crystal fiber. J. Opt. Soc. Am. B **27**(3), 592–598 (2010)
22. M. Erkintalo, G. Genty, J.M. Dudley, Giant dispersive wave generation through soliton collision. Opt. Lett. **35**(5), 658–660 (2010)
23. D.V. Skryabin, F. Luan, J.C. Knight, P.J. Russell, Soliton self-frequency shift cancellation in photonic crystal fibers. Science **301**(5640), 1705–1708 (2003)
24. L. Zhang, S.-G. Yang, Y. Han, H–.W. Chen, M–.H. Chen, S–.Z. Xie, Simultaneous generation of tunable giant dispersive waves in the visible and mid-infrared regions based on photonic crystal fibers. J. Opt. **15**(7), 075201 (2013)
25. L. Zhang, S. Yang, H. Chen, M. Chen, S. Xie, in Wavelength-tunable red-shift Cherenkov radiation in photonic crystal fibers for mid-infrared wavelength generation. *18th Opto-Electronics and Communications Conference, OECC*: 2013, WS4–4
26. J.M. Dudley, G. Genty, S. Coen, Supercontinuum generation in photonic crystal fiber. Rev. Mod. Phys. **78**(4), 1135 (2006)
27. J. Yuan, X. Sang, C. Yu, K. Wang, B. Yan, X. Shen, Y. Han, G. Zhou, S. Li, L. Hou, Widely wavelength-tunable two-colored solitons and small spectral component for broadband mid-infrared wavelength generation in a highly birefringent photonic crystal fiber. IEEE Photon. Technol. Lett. **24**(8), 670–672 (2012)
28. S.P. Stark, J.C. Travers, P.S.J. Russell, Extreme supercontinuum generation to the deep UV. Opt. Lett. **37**(5), 770–772 (2012)
29. T. Sylvestre, A.R. Ragueh, M.W. Lee, B. Stiller, G. Fanjoux, B. Barviau, A. Mussot, A. Kudlinski, Black-light continuum generation in a silica-core photonic crystal fiber. Opt. Lett. **37**(2), 130–132 (2012)
30. P.A. Champert, V. Couderc, P. Leproux, S. Février, V. Tombelaine, L. Labonté, P. Roy, C. Froehly, P. Nérin, White-light supercontinuum generation in normally dispersive optical fiber using original multi-wavelength pumping system. Opt. Express **12**(19), 4366–4371 (2004)
31. Y. Han, L.-T. Hou, J.-H. Yuan, C.-M. Xia, G.-Y. Zhou, Ultraviolet continuum generation in the fundamental mode of photonic crystal fibers. Chin. Phys. Lett. **29**(1), 014201 (2012)
32. L. Zhang, S. Yang, H. Chen, M. Chen, S. Xie, in Ultraviolet-shift supercontinuum generation by cross-phase modulation in photonic crystal fiber. *Conference on Lasers and Electro-Optics: Laser Science to Photonic Applications, CLEO*: 2013, JW2A.13

http://www.springer.com/978-3-662-48359-6

Ultra-Broadly Tunable Light Sources Based on the Nonlinear Effects in Photonic Crystal Fibers

Zhang, L.

2016, XIV, 94 p., Hardcover
ISBN: 978-3-662-48359-6